Ultrathin ambipolar polyelectrolyte capacitors prepared via layer-by-layer assembling

Alessandro Paghi[1], Stefano Mariani[1], Martina Corsi[1], Elena Maurina[1], Aline Debrassi[2], Lars Dähne[2], Simone Capaccioli[3,4], and Giuseppe Barillaro[1,4*]

[1]Dipartimento di Ingegneria dell'Informazione, Università di Pisa, via G. Caruso 16, 56122 Pisa, Italy.

[2]Surflay Nanotec GmbH, Max-Planck-Straße 3, 12489 Berlin, Germany.

[3]Physics Department, University of Pisa, Largo Pontecorvo 3, I-56127 Pisa, Italy.

[4]CISUP, Centro per l'Integrazione della Strumentazione dell'Università di Pisa, Lungarno Pacinotti 43, I-56126 Pisa, Italy.

[*]corresponding author: giuseppe.barillaro@unipi.it

Abstract

Miniaturized solid state capacitors leveraging migration of unipolar ions in a single polyelectrolyte layer sandwiched between metal electrodes, namely, polyelectrolyte capacitors (PECs), have been recently reported with areal capacitance up to 100-200 nF mm^{-2}. Nonetheless, application of PECs in consumer and industrial electronics has been hindered so far by their small operational frequency range, up to a few kHz, due to the resistive behavior (phase angle >-45°) of PECs in the range kHz-to-MHz.

Here we report on multilayer polyelectrolyte capacitors (mPECs) that leverage as dielectrics an ambipolar nanometer-thick (down to 10 nm) stack of anionic and cationic polyelectrolytes

assembled layer-by-layer between metal electrodes to eliminate the resistive behavior at frequencies from kHz to MHz. This significantly extends the operational range of mPECs over PECs. Specifically, mPECs with areal capacitance as high as 25 nF mm^{-2} at 20 Hz and full capacitive behavior from 10 mHz to 10 MHz are demonstrated using different assembling conditions and anionic/cationic polyelectrolyte pairs. The mPECs reliably operate over time for >300 million cycles, at different biasing voltages up to 3V and temperatures up to 80 °C, showing a reversible capacitive behavior without significant hysteresis.
Application of mPECs in flexible electronics operating at high frequency is envisaged.

Keywords
Multilayer, polyelectrolyte, capacitor, layer by layer (LbL), electrical double layer (EDL), ionic relaxation, ionic conductivity.

Introduction

Miniaturized solid state capacitors with high areal capacitance and large frequency range have been of interest for a wide variety of industrial, biomedical, and consumer electronic applications [1][2][3]. Recently, polyelectrolyte capacitors (PECs) with tremendous capacitance density (up to 100-200 nF mm^{-2}) were prepared by spin coating of polyelectrolyte monolayers with thickness >50 nm, leveraging the formation of an electrical double layer (EDL) at the polyelectrolyte/metal interface [4][5][6][7]. However, operation of current PECs is limited to low frequencies (typically up to a few kHz) because of their resistive behavior (phase angle >-45°) at frequencies in the kHz-to-MHz range (see Table S1). Unipolar free counterions oscillating forth and back in the material without reaching the metal electrodes are mainly responsible for resistive losses in this frequency range due to poor ion mobility and large thickness of polyelectrolytes used in PECs. Thus, possible strategies to push resistive losses at higher frequencies are improving ion mobility and/or decreasing the polyelectrolyte thickness. However, ion mobility of polyelectrolyte films used in

PECs does not change significantly in dry conditions, while reliable preparation of polyelectrolyte films by spin coating and/or drop casting becomes challenging when the thickness of the layer reduces below 50 nm (Table S1).

Multilayer assembling of polyelectrolytes and ionelastomers offers increased flexibility in tuning the functional properties of the resulting thin film, compared to a single layer, enabling material multifunctionalities that are difficult to achieve otherwise [8][9][10]. A micrometer-thick bilayer of anionic and cationic elastomers was prepared by injection molding and used to fabricate a *pn*-like semiconductor junction, which enabled the manufacturing of ionic logic circuit elements including diodes and transistors [8]. A similar architecture was proposed for the preparation of an electro-adhesive tape operating at a bias voltage as low as 1 V, featuring either strong or no adhesion in reverse and forward biasing, respectively, thanks to the formation and destruction of a large electric field across the ionelastomer junction due to migration of counterions [9]. A stack of thousands of bilayer cells of oppositely charged polyelectrolytes deposited combining drop casting and spray coating techniques was recently used to fabricate a power source with output voltage up to 1 kV under ambient conditions, namely, 25% RH, 25 °C. The voltage is generated by the spontaneous adsorption of water molecules from air and induced diffusion of oppositely-charged ions within the polyelectrolyte stack [10]. Yet, the thickness of the single layer in the multilayer stacks discussed above is in the μm range.

Layer-by-layer (LbL) assembling of polymers, colloids, biomolecules, and cells to form multilayer thin films offers superior reliability and better control of the film properties (thickness, charge, density) when compared to other deposition techniques, such as, spin coating, drop casting, and spray coating, especially for micro- and nano- structured materials [11]. Multilayer stacks have been successfully prepared via LbL with thickness of few nm up to several μm [11][12] and employed in different research fields, including separation science [13][14], drug delivery [15][16][17][18], bio-medicine and -sensing [19][20][21][22][23][24], electronics [25]. However, the use of nm-thick polyelectrolyte multilayers as dielectric material for the preparation of solid-

state capacitors has been overlooked so far, and only a few studies on the dielectric behavior of polyelectrolyte stacks versus assembling condition, material, temperature, and humidity have been performed using electrooptical methods [26][27][28][29], impedance spectroscopy [30][31], and DC-conductivity evaluation [32].

Here, we report on multilayer polyelectrolyte capacitors (mPECs) that leverage as dielectrics an ambipolar nanometer-thick (down to 10 nm) stack of anionic and cationic polyelectrolytes assembled layer-by-layer between metal electrodes. The mPEC areal capacitance is as high as 25 nF mm^{-2} at 20 Hz for the 10-nm-thick multilayer stack (10 anionic/cationic bilayers), which is comparable to most of PECs fabricated via spin-coating and drop-casting reported in the literature [4][33][34][35][36][37]. The mPEC architecture does not show any resistive range thanks to the ambipolar nature of the polyelectrolyte stack and keeps a full capacitive behavior from 10 mHz to 10 MHz, thus extending the operational range compared to PECs. The mPEC reliably operates over time for >300 million cycles, at different biasing voltages up to 3V and temperatures up to 80 °C, exhibiting a reversible capacitive behavior without significant hysteresis. Further, we show that different assembling conditions and polyelectrolyte pairs can be used to prepare mPECs with similar capacitive behavior, thus pointing out the robustness and flexibility of the method.

Results and discussion

mPECs are fabricated layer by layer via repetitive electrostatic assembling of two polyelectrolytes with opposite charge, as depicted in Figure 1a.

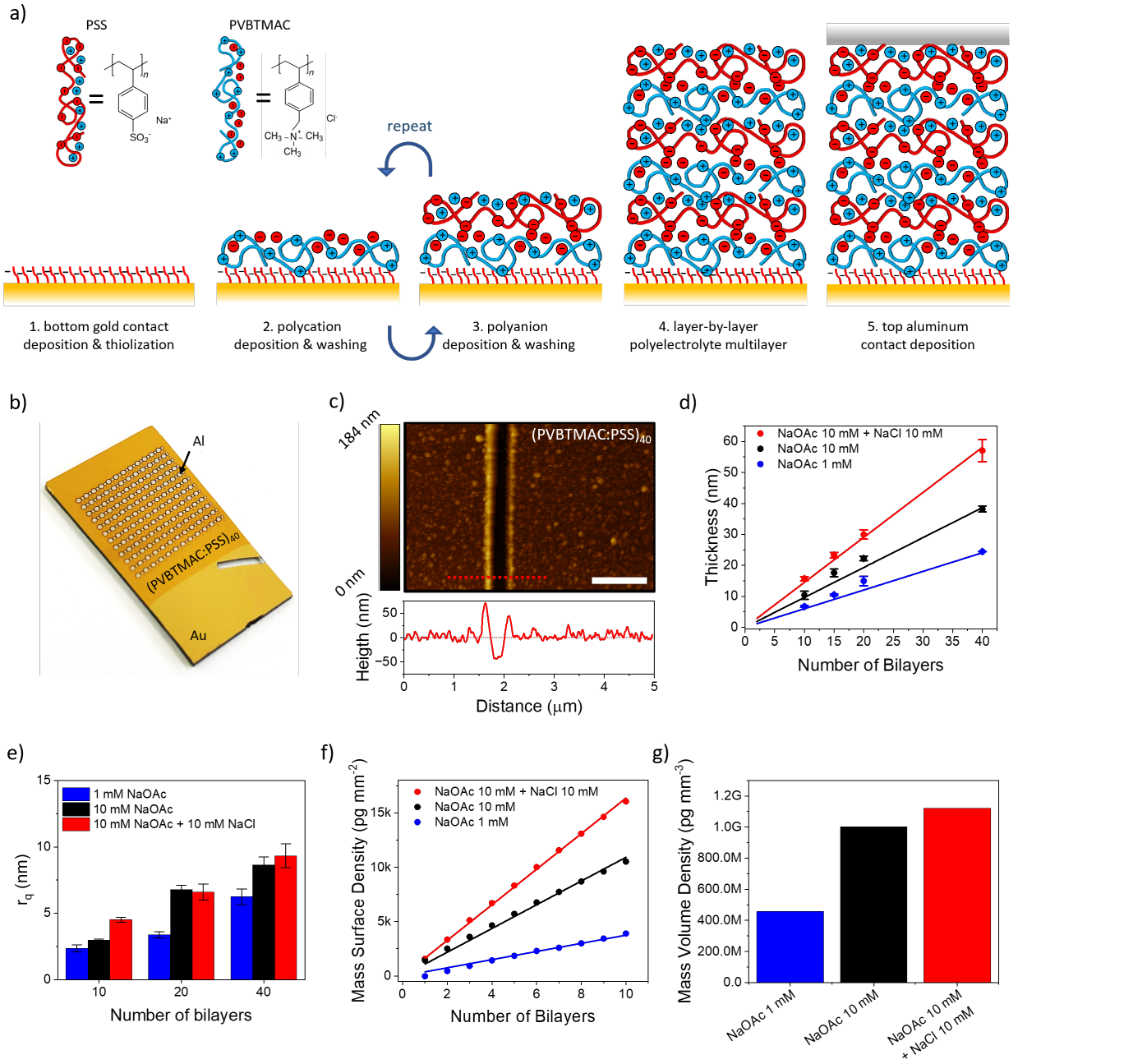

Figure 1: Fabrication and morphological characterization of mPECs. (a) Main preparation steps of mPECs: (1) Bottom gold contact deposition and thiol functionalization. The gold surface is provided with a net negative charge; (2) Polycation deposition and washing. The surface is provided with a net positive charge; (3) Polyanion deposition and washing. The surface is provided with a net negative charge; (4) Steps (2) and (3) are repeated as needed to reach the final polyelectrolyte multilayer configuration/number of bilayers; (5) Top aluminum contact deposition. (b) Top-view picture of an array of mPECs with 40 bilayers and different diameters. (c) Top: AFM image (tip-scratched) of a polyelectrolyte stack with 40 bilayers of PVTBMAC:PSS. Scalebar is 1μm; Bottom: Height profile across the scratch line highlighting the multilayer thickness. (d) Thickness, (e) root mean square roughness, and (f) mass surface density values of PVTBMAC:PSS stacks with different number of bilayers and in different assembling conditions. g) Mass volume density values of PVTBMAC:PSS stacks prepared with different assembling conditions. Data in d), e) are reported as the average value measured over 3 mPECs for each number of bilayers, with error bars representing the standard deviation.

A gold-coated glass slide is functionalized with 11-mercaptoundecanoic acid (MUA) to provide the surface with a negative charge (Figure 1a.1) [38]. Then, a multilayer stack of nanometer-thick polyelectrolytes, namely, the positively-charged poly(vinyl benzyl trimethylammonium chloride) (PVBTMAC:Cl) [39] and negatively-charged sodium poly(styrene sulfonate) (PSS:Na) [40], is assembled layer by layer on the gold-coated slide leveraging electrostatic interactions (Figure 1a.2-3). Polyelectrolyte stacks with a different number of bilayers are explored, namely, 10, 20, and 40 (Figure 1a.4). Aluminum dots (a 12 × 12 array) with diameter of 50 to 400 μm are eventually patterned on top of the polyelectrolyte stack to provide independent electrodes for the capacitors; the gold layer beneath the MUA serves as the common bottom electrode of all the capacitors (Figure 1a.5). The choice of aluminum as top electrode is due to its lower cost compared to gold; indeed, we do not expect any significant dependence of the mPEC performance on the top metal electrode.

The polyelectrolyte stack is assembled through cyclic dip-coating of the MUA-functionalized slab in aqueous solutions of PVBTMAC:Cl and PSS:Na, both with concentration of 1 mg/ml in sodium acetate (NaOAc) buffer at pH 5.5 and room temperature (21°C, RT). Both the polyelectrolytes are soluble in water, which guarantees a strong polymer dissociation in aqueous solution and, in turn, a large positive charge for $PVBTMAC^{+}:Cl^{-}$ thanks to the presence of quaternary ammonium cation-based monomers [39], and negative charge for the $PSS^{-}:Na^{+}$ thanks to the low pKa value (i.e., 1.95) [41]. Besides electrostatic interactions between the oppositely-charged polyeelctrolytes, π–π interactions between the aromatic rings of the vinyl-benzyl group of PVBTMAC:Cl and the styrene group of PSS:Na further improve stabilization of the assembled multilayer stack [42][43][44]. Figure 1b shows an optical picture of the as-fabricate array of mPECs with a polyelectrolyte stack of 40 bilayers. An atomic force microscopy (AFM) top-view image of the polyelectrolyte stack with 40 bilayer is shown in Figure 1c, from which height profile and surface roughness value are extrapolated. Thickness of the polyelectrolyte stack *vs.* number of bilayers assembled in different

buffer conditions are given in Figure 1d, measured using both ellipsometry and AFM (Figure S1). A linear increment of the multilayer thickness with the number of bilayers is observed, regardless of the assembling buffer; the higher the ionic strength of the buffer the larger the thickness of the stack for a given number of layers, due to the increased folding of the polyelectrolytes deposited on the surface as the ionic strength increases. Best fitting of data in Figure 1d with a linear function results in a growth rate ranging from 0.60 and 1.45 nm bilayer^{-1} in 1 mM NaOAc and 10 mM NaOAc:10 mM NaCl buffers, respectively. Roughness increases from 5 to 10 nm with the number of bilayers for the tested buffers (Figure 1e), which is in agreement with values reported in the literature on polyelectrolytes stacks [45][46]. The roughness/thickness ratio is between ~0.3 and ~0.2, and tends to reduce as the thickness of the stack increases. The assembling process was further investigated by real-time whispering gallery mode (WGM) and quartz microbalance (QCM) analysis (Figure S2, S3) [47]. The polymer deposition stabilizes in few tens of seconds, with no significant polymer mass loss during the rinsing phase. A linear increment of the mass surface density with the deposition time and, in turn, with the number of bilayers is observed (Figure 1f), with an experimental PVBTMAC/PSS charge density ratio of 1.1:1 that is in agreement with the theoretical PVBTMAC/PSS value of 1.1:1. Also in this case, the higher the ionic strength of the buffer the larger the mass surface density increase for a given number of layers, namely, from 375 to 1636 pg mm^{-2} bilayer^{-1} using 1 mM NaOAc and 10 mM NaOAc:10 mM NaCl buffers, respectively (Figure S2d).

Figure 1g shows mass volume density values of polyelectrolyte stacks prepared in the different assembling buffers, as obtained from thickness and mass surface density data in Figure 1d,f. Densities of about 1×10^{9} pg mm^{-3} are achieved in 10 mM NaOAc buffers that are comparable to those of common polymers, such as poly(styrene) [48], and polymer stacks deposited by LbL technique [49,50]; on the other hand, a lower density of 0.46 pg mm^{-3} is achieved using 1 mM NaOAc as the assembling buffer. In fact, as the ionic strength increases, the polymers assume a more coiled conformation, thus occupying a lower surface area per unit chain [51].

We next investigated the electrical performance over frequency in air at RT of the mPECs fabricated with multilayer stacks of PVBTMAC:PSS with a number of bilayers ranging from 10 to 40. We note that the minimum number of bilayers ensuring reliable dielectric insulation between top (Al) and bottom (Au) electrodes is 10, regardless of the chosen buffer. All the devices showed a full capacitive behavior over frequency, with best performance in terms of areal capacitance achieved for the 10 mM NaOAc buffer (Figure 2a and S4). In the following we will focus on the results achieved for mPECs prepared in 10 mM NaOAc buffer, unless otherwise stated.

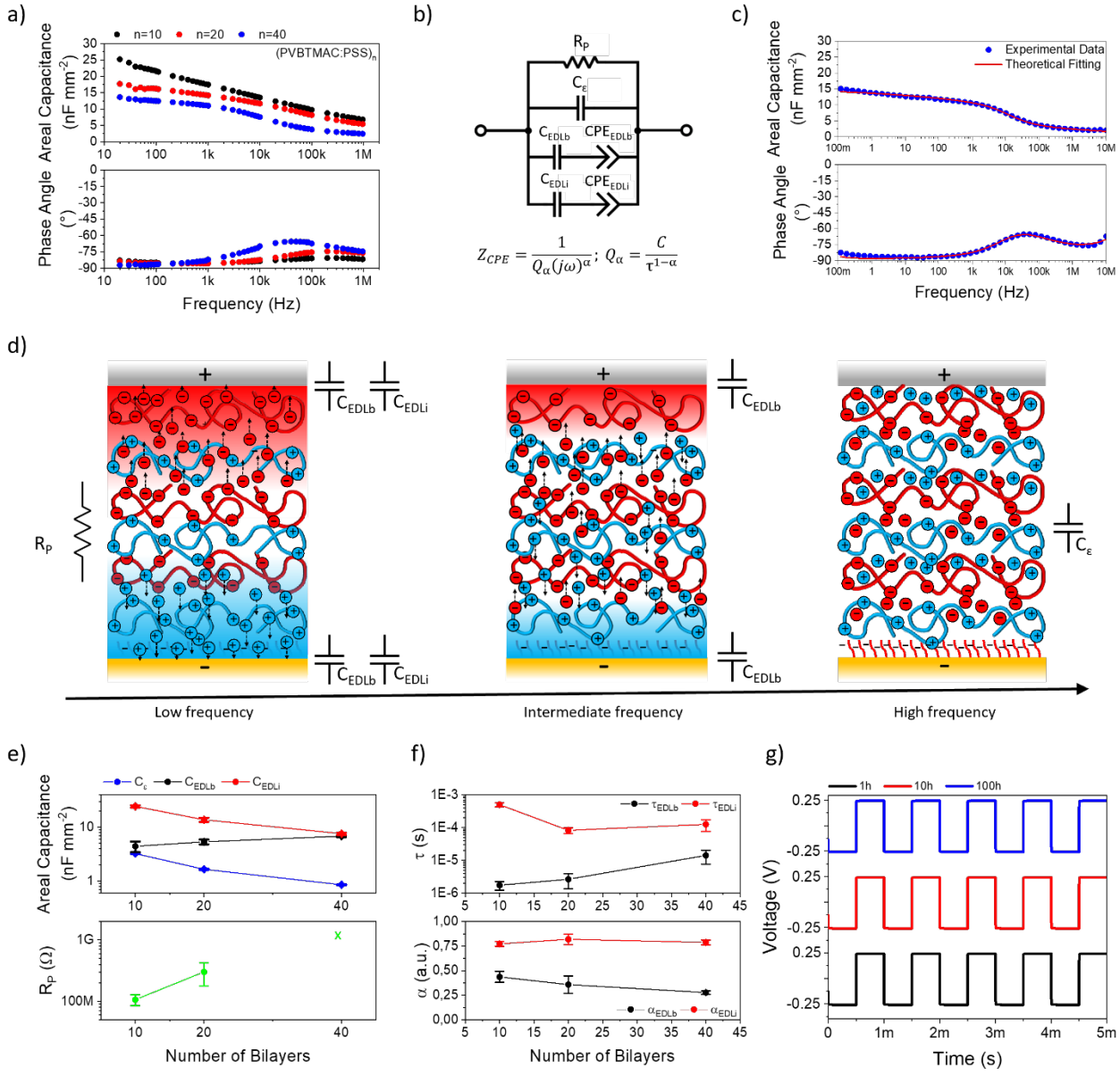

Figure 2: Electrical characterization of mPECs. (a) Areal capacitance and phase angle curves vs. frequency of mPECs prepared with a different number of PVTBMAC:PSS bilayers in 10 mM

NaOAc buffer. (b) Theoretical lumped model of mPECs, used to best-fit experimental data. (c) Experimental data superposed to best-fitting curves of areal capacitance and phase angle of mPEC with 40 bilayers of PVTBMAC:PSS over an extended frequency range of 100 mHz to 10 MHz. (d) Schematic illustration of mPECs showing charge configuration of anionic and cationic polyelectrolytes in the multilayer stack over frequency. At low frequency, EDLs are formed at the polyelectrolyte/electrode interfaces thanks to accumulation of free counterions (C_{EDLi}) and depletion of polyelectrolyte backbones (C_{EDLb}); at intermediate frequency, only depletion of backbones from free counterions contribute to EDL formation; at high frequency, EDL formation does not occur and dielectric polarization rules to mPEC behavior. (e,f) Lumped circuit parameter values (capacitance, resistance, relaxation time, distribution coefficient) of mPECs with different number of PVTBMAC:PSS bilayers, as achieved from best-fitting of experimental data in (a). (g) Charge/discharge cycles at 1 kHz of mPECs with 20 bilayers of PVTBMAC:PSS over 100 hours of continuous operation. The symbol "x" in e) means that R_p is above the maximum value measurable with the system (> 1GΩ). Data in e) and f) are reported as the average value measured over 3 mPECs for each number of bilayers, with error bars representing the standard deviation.

Figure 2a shows frequency-resolved areal capacitance and phase angle measured on mPECs with 10, 20, and 40 bilayers and top contact of 200 µm in diameter.

The capacitance value reduces with the number of bilayers and over frequency, as expected, from 25.2 nF mm^{-2} at 20 Hz (10 bilayers) to 13.7 nF mm^{-2} for 40 bilayers (20 Hz), and 6.8 nF mm^{-2} at 1 MHz (10 bilayers); remarkably, the phase angle keeps staying always below -65° and mostly close to -90° over the whole frequency range, thus ensuring a fully capacitive behavior of the device from 20 Hz to 1MHz. Similar results are also achieved for mPECs with 400 µm in diameter both in terms of areal capacitance and phase angle values, thus confirming the robustness of mPECs (Figure S5). This latter result is of major importance as it states that it is possible to increase/decrease the overall capacitance value tuning the size of mPECs, keeping mPECs performance unchanged in terms of areal capacitance and phase angle values.

mPECs show a significant improvement in terms of capacitive range over frequency, when compared to common bulk polyelectrolyte capacitors fabricated by spin-coating and drop-casting for which typically two frequency decades of resistive behavior are usually observed (see Table S1) (i.e., capacitive behavior if the phase angle is < -45 °, resistive behavior if phase angle is > -45 °).

The extension of the capacitive range occurs with a reduction the areal capacitance at low

frequencies compared to best PECs, though the values become comparable when the operation frequency is increased at 1 MHz.

We assume that the behavior of mPECs over frequency is ruled out by, namely, dielectric polarization of the polyelectrolyte stack at frequencies > 300 kHz; ionic relaxation of dissociated cations Na^+ of PSS and anions Cl^- of PVBTMAC at frequencies between 10 kHz and 300 kHz; formation of EDL at the polyelectrolyte/electrode interfaces at frequencies <10 kHz. We notice that ionic relaxation at intermediate frequencies is more pronounced and shifts to lower frequencies as the number of bilayers in the polyelectrolyte stack increases (Figure 2a, bottom). Notice that the polarization mechanisms accounted above are commonly accepted for PECs, are reported for polyelectrolyte capacitor based on PSS [5,52], poly(vinyl phosphonic acid-*co*-acrylic acid) P(VPA-AA) [4,53], and poly[(1-vinylpyrrolidone)-*co*-(2-ethyldimethylammonioethyl methacrylate ethyl sulfate)] (P(VP-EDMAEMAES)) [4].

Based on the assumptions above, we modeled the mPEC with the lumped electrical circuit shown in Figure 2b, then we used it to best-fit frequency-resolved data. The multilayer stack is considered as a homogeneous dielectric material due to the sub-nanometric thickness (about 0.5 nm) (Figure 1d) and the strong interpenetration (about 50-60 % of the layer thickness) of the two polyelectrolytes [40,54]. The circuit consists of a resistor R_p modeling ohmic losses at zero frequency and a capacitor C_ε modeling dielectric polarization of the entire polyelectrolyte stack at high frequency. A branch containing a constant phase element (CPE_{EDLi}) and a capacitor (C_{EDLi}) considers migration of Na^+ and Cl^- counterions contributing to the formation of EDLs at the two metal electrodes, under biasing. In our case, Na^+ ions migrate towards the negatively charged electrode, while the opposite occurs for Cl^- ions. A further branch consisting of a constant phase element (CPE_{EDLb}) and a capacitor (C_{EDLb}) considers the contribution to EDLs of ion-depleted polycation and polyanion backbones in the multilayer stack, caused by counterion migration. The capacitors at the two electrodes are not expected to be identical, since the spatial distribution of the Na^+ and Cl^- ions, as well as that of PSS^- and $PVBTMAC^+$ backbones are expected to differ at the two interfaces.

We assume that polyelectrolytes in the stack close to the electrodes are quickly depleted of their counterions upon application of an oscillating electric field, so that ion-depleted backbones contribute to the formation of EDLs up to intermediate frequencies (Figure 2d, center). Conversely, ion migration is expected to contribute to EDLs formed at the electrodes at lower frequencies, when the temporal period of the oscillating field is long enough to allow the ions travelling through the multilayer stack to enrich EDLs formed at the electrodes (Figure 2d, left). Dielectric polarization of the entire polyelectrolyte stack occurs at high frequency (Figure 2d, right). Two Cole-Cole branches are used to model the two processes above, with the CPE impedance being schematized as $Z_{CPE} = \frac{1}{Q_\alpha (j\omega)^\alpha}$, with $Q_\alpha = \frac{C}{\tau^{1-\alpha}}$ and $0 \leq \alpha \leq 1$, and depending on the characteristic relaxation time (τ) and distribution coefficient (α) of the processes. Similar lumped models have been used to fit frequency-resolved areal capacitance and phase angle data of spin-coated PECs [5,34], though using a single ionic relaxation process to take into account oscillation of a single type of counterion, e.g., H^+ in PSS:H [5] and P(VPA-AA):H [4].

Best-fitting of experimental data of mPECs with the proposed model results in an excellent agreement over the whole range 20 Hz to 1MHz, regardless of the number of layers of the polyelectrolyte stack (Figure S6). The use of an extended frequency range from 100 mHz to 10MHz further confirms the validity of the proposed model (Figure 2c). A maximum series resistance of 35 Ω is extracted for the mPEC with 40 bilayers, whereas R_p increases from 0.1 to more than 1 GΩ (not measurable) from 10 to 40 bilayers thanks to reduced ohmic losses as the polyelectrolyte stack thickness increases (Figure 2e, bottom). On the other hand, C_ε reduces from 3.23 to 0.85 nF mm^{-2} with the number of bilayers as theoretically expected, and C_{EDLi} follows a similar trend reducing from 24.5 nFmm^{-2} to about 6 nFmm^{-2}; conversely, C_{EDLb} has a roughly constant value of about 4.5 to 6 nFmm^{-2} (Figure 2e, top).

Correct assignment of C_{EDLb}-CPE_{EDLb} and C_{EDLi}-CPE_{EDLi} branches to EDLs formed by polymer backbone and free counterions at the electrodes, respectively, is supported by relaxation time and

distribution coefficient values. CPE_{EDLb} has a faster relaxation time τ_{EDLb} (1 to 10 μs) that is one order of magnitude (at least) lower than τ_{EDLi} (0.1 to 1 ms) of CPE_{EDLi} (Figure 2f, top). Further, CPE_{EDLi} exhibits a more capacitive behavior compared to CPE_{EDLb} (α_{EDLi}~$3\alpha_{EDLb}$) thanks to the higher mobility of counterions with respect to the fixed polymer backbones (Figure 2f, bottom). The reduction of C_{EDLi} with the multilayer thickness is consistent with the decrease of counterion velocity, which results in a smaller number of ions reaching the electrodes to form the EDL in a given time (frequency). In fact, the electric field strength E reduces as the thickness d of the multilayer stack increases ($E=V/d$), so does the ion velocity v_i ($v_i=\mu_i E$, with μ_i the counterions mobility), for a given applied voltage V. On the other hand, the C_{EDLb} is not expected to be thickness-dependent, given that ion-depleted backbones of polyelectrolytes close to the metal electrodes are mainly contributing to EDL formation.

We next evaluated the behavior of mPECs fabricated with 20 bilayers over 100 h of continuous operation in air at RT, upon application of a square-wave signal with peak-to-peak voltage of 0.5 V and frequency of 1 kHz (i.e., 3.6×10^8 charging/discharging cycles). Figure 2g shows charge/discharge cycles of the mPEC after 1 h, 10 h, and 100 h of operation. A good reliability of the capacitor is apparent over time, with no significant aging effects. By best-fitting experimental charge/discharge transient curves (Figure S7a), a rise time variation <15 % over 100 h of continuous operation is observed (Figure S7b).

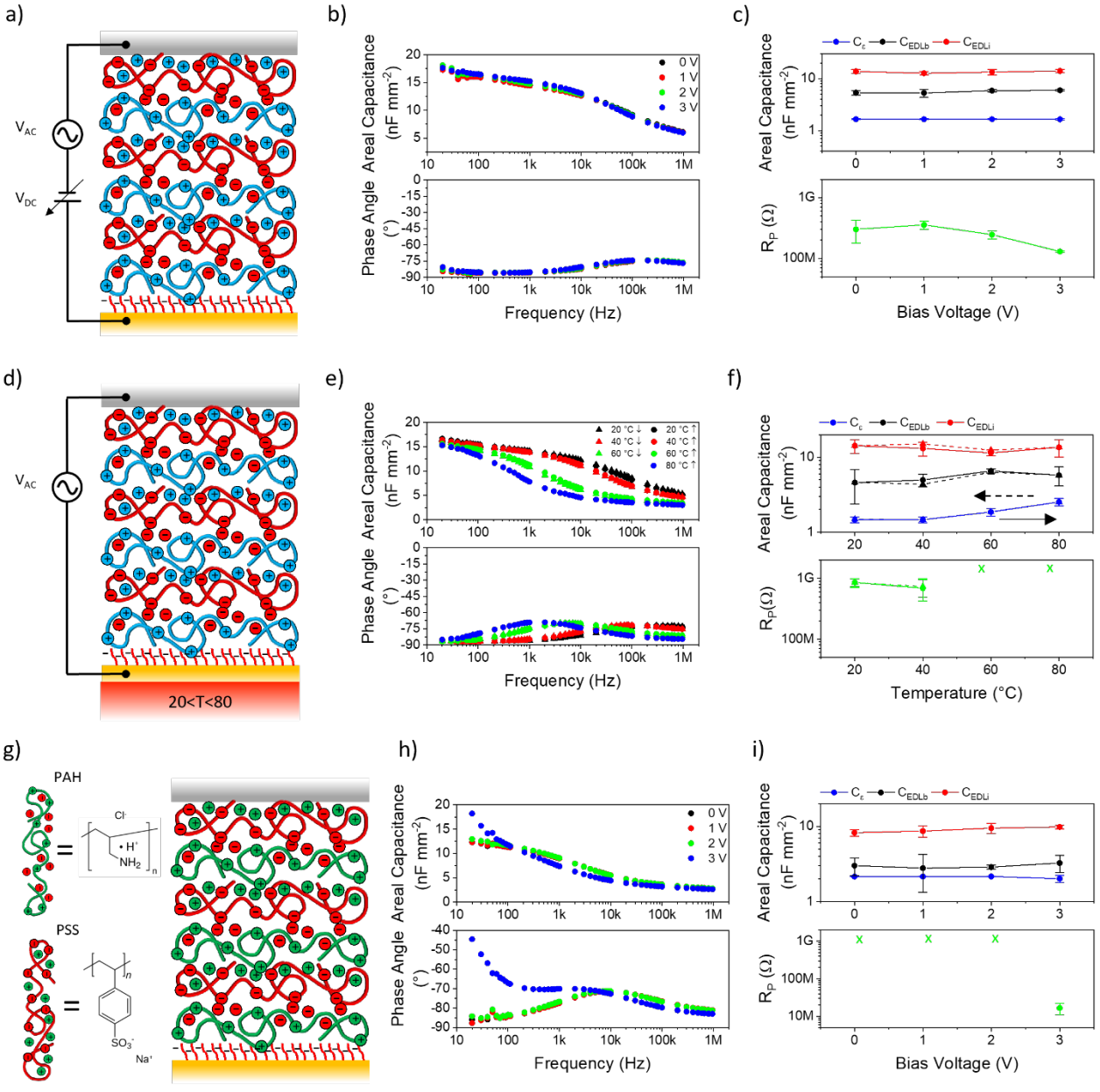

Figure 3: Electrical characterization of mPECs vs. voltage, temperature, and polyelectrolytes. (a) Sketch of mPEC operated at different bias voltages. (b) Areal capacitance and phase angle curves vs. frequency at different bias voltages of mPEC fabricated with 20 bilayers of PVTBMAC:PSS. (c) Areal capacitance and resistance values vs. bias voltage as achieved from best fitting of experimental data in (b). (d) Sketch of mPEC operated at different temperatures. (e) Areal capacitance and phase angle curves vs. frequency at different temperatures of mPEC fabricated with 20 bilayers of PVTBMAC:PSS. Solid (dashed) traces indicate temperature is rising up (cooling down). (f) Areal capacitance and resistance values vs. bias voltage as achieved from best fitting of experimental data in (e). (g) Sketch of mPEC with a polyelectrolyte stack of PAH:PSS; the green polymer represents PAH:Cl and the red one is PSS:Na. (h) Areal capacitance and phase angle curves vs. frequency at different bias voltages of mPEC fabricated with 20 bilayers of PAH:PSS. (i) Areal capacitance and resistance values vs. bias voltage as achieved from best fitting of experimental data in (h). The symbol "x" in f), g) means that R_p is above the maximum value measurable with the system (> 1GΩ). Data in c), f), i) are reported as the average value measured over 3 mPECs for each bias voltage and temperature, with error bars representing the standard deviation.

We then investigated the behavior of mPECs at different bias voltages in the range 0-3 V (Figure 3a). Both areal capacitance and phase angle were measured over the frequency range 20 Hz through 1 MHz in air at RT at increasing bias values. Figure 3b shows areal capacitance and phase angle curves for mPECs with 20 bilayers. No significant variation is apparent with the bias voltage. This is confirmed by best-fitting parameters, which are constant with the bias voltage (Figure 3c and S8). A slight reduction of R_p is observed with the bias voltage, which is consistent with increased leakage of the polyelectrolyte stack (Figure 3c bottom). Similar results were obtained also for mPECs fabricated with both 10 and 40 bilayers (Figure S9). We note that, an increase of the bias voltage above 3 V results in the breakdown of the multilayer stack.

Next, we investigated the behavior of mPECs at different temperatures in the range 20-80 °C (Figure 3d). The electrical impedance was measured in air at different temperatures, both upward and downward, in the frequency range 20 Hz-1 MHz and constant bias voltage of 0 V. A time delay of 1 hour between two consecutive measurements was set to ensure the ionic conductivity reached a steady state value at the new temperature upon adsorption/desorption of water in/from the multilayer stack [55]. Figure 3e shows areal capacitance and phase angle curves measured upon variation of the temperature from 20 to 80 °C (and back) on mPECs with 20 bilayers. C_ε, C_{EDLb}, and C_{EDLi} values are rather constant over temperature (Figure 3f). The phase angle stays below -65 ° regardless of the temperature value, confirming a full capacitive behavior over the whole frequency range. A progressive shift of the relaxation peak toward lower frequencies is observed as the temperature increases, which is consistent with an increase of the process relaxation times, namely, τ_{EDLb} from 1 μs to 500 μs and τ_{EDLi} from 40 μs to 200 ms (Figure S10), due to progressive dehydration of the polyelectrolyte stack as the temperature increase, which reduces the counterion mobility [5]. The mPECs show an excellent superposition of upward and downward scans, indication of a fully reversible behavior with temperature, with no hysteresis (Figure 3e,f).

Eventually, to demonstrate flexibility of the approach, we used a different polyelectrolyte pairs for the preparation of a mPEC with 20 bilayers, namely, the negatively-charged PSS:Na and the

positively-charged poly(allylamine hydrochloride) (PAH:Cl) (Figure 3g). Figure S11a shows an AFM top-view image of a tip-scratched polyelectrolyte multilayer stack, from which a thickness of 28.8 ± 0.9 nm and a root mean square roughness of 2.99 ± 0.7 nm are extrapolated for the multilayer stack. Areal capacitance and phase angle curves measured at RT for different bias voltages of the PSS:Na/PAH:Cl mPEC are shown in Figure 3h. The behavior of the mPEC looks like that of the PSS:Na/PVBTMAC:Cl mPEC with 20 bilayers, though with a slightly smaller areal capacitance, as confirmed by the values of C_{ε}, C_{EDLb}, C_{EDLi} achieved by best fitting experimental data. The phase angle is always below -65° over the whole frequency range, though the relaxation frequency of the polyelectrolyte multilayer is shifted at lower frequency, as confirmed by value of the relaxation times (Figure S10b). The behavior with the bias voltage is also similar between PSS:Na/PAH:Cl and PSS:Na/PVBTMAC:Cl mPECs, with parameters of the lumped model being not significantly affected, except for a reduction of R_P at 3 V, beyond which dielectric breakdown occurs.

Conclusions

In this work we report on the preparation of ambipolar multilayer polyelectrolyte capacitors (mPECs) leveraging the layer-by-layer deposition of a nanometer thick (down to 10 nm) stack of anionic and cationic polyelectrolytes - between metal electrodes - as dielectric material. mPECs show a full capacitive behavior from 10 mHz to 10 MHz, eliminating the typical resistive behavior in the range kHz to MHz typical of PECs and enabling, in turn, the use of polyelectrolyte capacitors in most of industrial and consumer electronic applications. mPECs with areal capacitance around 20 nF mm^{-2} are reliably prepared using different assembling conditions and polyelectrolyte pairs, with reliable operation over time, at different biasing voltages up to 3V and temperatures up to 80 °C, without significant hysteresis.

Building up on these results, the use of ambipolar nanometer-thick polyelectrolyte dielectrics for the preparation of flexible electronic devices operating at high frequency, among which capacitors and

field effect transistors, can be envisaged, leveraging the vast number of anionic and cationic polyelectrolytes available on the market.

Acknowledgments

This work was partially supported by the FoReLab project, funded by the Italian Ministry of Education under the programme "Dipartimenti di Eccellenza".

References

[1] D. Qi, Y. Liu, Z. Liu, L. Zhang, X. Chen, Design of Architectures and Materials in In-Plane Micro-supercapacitors: Current Status and Future Challenges, Adv. Mater. 29 (2017) 1–19. https://doi.org/10.1002/adma.201602802.

[2] L. Strambini, A. Paghi, S. Mariani, A. Sood, J. Kalliomäki, P. Järvinen, F. Toia, M. Scurati, M. Morelli, A. Lamperti, G. Barillaro, Three-dimensional silicon-integrated capacitor with unprecedented areal capacitance for on-chip energy storage, Nano Energy. 68 (2020) 104281. https://doi.org/10.1016/j.nanoen.2019.104281.

[3] P. Banerjee, I. Perez, L. Henn-Lecordier, S.B. Lee, G.W. Rubloff, Nanotubular metal-insulator-metal capacitor arrays for energy storage, Nat. Nanotechnol. 4 (2009) 292–296. https://doi.org/10.1038/nnano.2009.37.

[4] L. Herlogsson, X. Crispin, S. Tierney, M. Berggren, Polyelectrolyte-gated organic complementary circuits operating at low power and voltage, Adv. Mater. 23 (2011) 4684–4689. https://doi.org/10.1002/adma.201101757.

[5] O. Larsson, E. Said, M. Berggren, X. Crispin, Insulator polarization mechanisms in polyelectrolyte-gated organic field-effect transistors, Adv. Funct. Mater. 19 (2009) 3334–3341. https://doi.org/10.1002/adfm.200900588.

[6] L. Herlogsson, X. Crispin, N.D. Robinson, M. Sandberg, O.J. Hagel, G. Gustafsson, M. Berggren, Low-voltage polymer field-effect transistors gated via a proton conductor, Adv.

Mater. 19 (2007) 97–101. https://doi.org/10.1002/adma.200600871.

[7] E. Said, X. Crispin, L. Herlogsson, S. Elhag, N.D. Robinson, M. Berggren, Polymer field-effect transistor gated via a poly(styrenesulfonic acid) thin film, Appl. Phys. Lett. 89 (2006) 10–13. https://doi.org/10.1063/1.2358315.

[8] H.J. Kim, B. Chen, Z. Suo, R.C. Hayward, Ionoelastomer junctions between polymer networks of fixed anions and cations, Science (80-.). 367 (2020) 773–776. https://doi.org/10.1126/science.aay8467.

[9] H.J. Kim, L. Paquin, C.W. Barney, S. So, B. Chen, Z. Suo, A.J. Crosby, R.C. Hayward, Low-Voltage Reversible Electroadhesion of Ionoelastomer Junctions, Adv. Mater. 32 (2020) 2000600. https://doi.org/10.1002/adma.202000600.

[10] H. Wang, Y. Sun, T. He, Y. Huang, H. Cheng, C. Li, D. Xie, P. Yang, Y. Zhang, L. Qu, Bilayer of polyelectrolyte films for spontaneous power generation in air up to an integrated 1,000 V output, Nat. Nanotechnol. 16 (2021) 811–819. https://doi.org/10.1038/s41565-021-00903-6.

[11] J.J. Richardson, J. Cui, M. Björnmalm, J.A. Braunger, H. Ejima, F. Caruso, Innovation in Layer-by-Layer Assembly, Chem. Rev. 116 (2016) 14828–14867. https://doi.org/10.1021/acs.chemrev.6b00627.

[12] Y. Li, X. Wang, J. Sun, Layer-by-layer assembly for rapid fabrication of thick polymeric films, Chem. Soc. Rev. 41 (2012) 5998. https://doi.org/10.1039/c2cs35107b.

[13] W. Jin, A. Toutianoush, B. Tieke, Use of polyelectrolyte layer-by-layer assemblies as nanofiltration and reverse osmosis membranes, Langmuir. 19 (2003) 2550–2553. https://doi.org/10.1021/la020926f.

[14] F. Paquin, J. Rivnay, A. Salleo, N. Stingelin, C. Silva, Multi-phase semicrystalline microstructures drive exciton dissociation in neat plastic semiconductors, J. Mater. Chem. C. 3 (2015) 10715–10722. https://doi.org/10.1039/b000000x.

[15] R.C. Smith, M. Riollano, A. Leung, P.T. Hammond, Layer-by-layer platform technology for

small-molecule delivery, Angew. Chemie - Int. Ed. 48 (2009) 8974–8977. https://doi.org/10.1002/anie.200902782.

[16] Y. Yan, G.K. Such, A.P.R. Johnston, H. Lomas, F. Caruso, Toward therapeutic delivery with layer-by-layer engineered particles, ACS Nano. 5 (2011) 4252–4257. https://doi.org/10.1021/nn201793f.

[17] B. Kim, S.W. Park, P.T. Hammond, Hydrogen-Bonding Layer-by-Layer-Assembled Biodegradable Polymeric Micelles as Drug Delivery Vehicles from Surfaces, ACS Nano. 2 (2008) 386–392. https://doi.org/10.1021/nn700408z.

[18] X. Su, B.-S. Kim, S.R. Kim, P.T. Hammond, D.J. Irvine, Layer-by-Layer-Assembled Multilayer Films for Transcutaneous Drug and Vaccine Delivery, ACS Nano. 3 (2009) 3719–3729. https://doi.org/10.1021/nn900928u.

[19] Z. Poon, D. Chang, X. Zhao, P.T. Hammond, Layer-by-layer nanoparticles with a pH-sheddable layer for in vivo targeting of tumor hypoxia, ACS Nano. 5 (2011) 4284–4292. https://doi.org/10.1021/nn200876f.

[20] S. Mariani, V. Robbiano, L.M. Strambini, A. Debrassi, G. Egri, L. Dähne, G. Barillaro, Layer-by-layer biofunctionalization of nanostructured porous silicon for high-sensitivity and high-selectivity label-free affinity biosensing, Nat. Commun. 9 (2018) 5256. https://doi.org/10.1038/s41467-018-07723-8.

[21] S. Mariani, A. Paghi, A.A. La Mattina, A. Debrassi, L. Dähne, G. Barillaro, Decoration of Porous Silicon with Gold Nanoparticles via Layer-by-Layer Nanoassembly for Interferometric and Hybrid Photonic/Plasmonic (Bio)sensing, ACS Appl. Mater. Interfaces. 11 (2019) 43731–43740. https://doi.org/10.1021/acsami.9b15737.

[22] M. Corsi, A. Paghi, S. Mariani, G. Golinelli, A. Debrassi, G. Egri, G. Leo, E. Vandini, A. Vilella, L. Dähne, D. Giuliani, G. Barillaro, Bioresorbable Nanostructured Chemical Sensor for Monitoring of pH Level In Vivo, Adv. Sci. 9 (2022) 2202062. https://doi.org/10.1002/advs.202202062.

[23] A. Paghi, M. Corsi, A.A. La Mattina, G. Egri, L. Dähne, G. Barillaro, Wireless and Flexible Optoelectronic System for In Situ Monitoring of Vaginal pH Using a Bioresorbable Fluorescence Sensor, Adv. Mater. Technol. 8 (2023). https://doi.org/10.1002/admt.202201600.

[24] C.S. Peyratout, L. Dähne, Tailor-Made Polyelectrolyte Microcapsules: From Multilayers to Smart Containers, Angew. Chemie Int. Ed. 43 (2004) 3762–3783. https://doi.org/10.1002/anie.200300568.

[25] A.-M. Pappa, S. Inal, K. Roy, Y. Zhang, C. Pitsalidis, A. Hama, J. Pas, G.G. Malliaras, R.M. Owens, Polyelectrolyte Layer-by-Layer Assembly on Organic Electrochemical Transistors, ACS Appl. Mater. Interfaces. 9 (2017) 10427–10434. https://doi.org/10.1021/acsami.6b15522.

[26] T. Radeva, V. Milkova, I. Petkanchin, Electrical properties of multilayers from low- and high-molecular-weight polyelectrolytes, J. Colloid Interface Sci. 279 (2004) 351–356. https://doi.org/10.1016/j.jcis.2004.06.078.

[27] T. Radeva, V. Milkova, I. Petkanchin, Dynamics of counterions in polyelectrolyte multilayers studied by electro-optics, Colloids Surfaces A Physicochem. Eng. Asp. 240 (2004) 27–34. https://doi.org/10.1016/j.colsurfa.2004.03.010.

[28] T. Radeva, M. Grozeva, In situ determination of thickness and electrical properties of multilayers from weak polyelectrolytes, J. Colloid Interface Sci. 287 (2005) 415–421. https://doi.org/10.1016/j.jcis.2005.02.016.

[29] V. Milkova, T. Radeva, Effect of ionic strength and molecular weight on electrical properties and thickness of polyelectrolyte bi-layers, Colloids Surfaces A Physicochem. Eng. Asp. 424 (2013) 52–58. https://doi.org/10.1016/j.colsurfa.2013.02.034.

[30] M.F. Durstock, M.F. Rubner, Dielectric Properties of Polyelectrolyte Multilayers, Langmuir. 17 (2001) 7865–7872. https://doi.org/10.1021/la010954i.

[31] D.M. DeLongchamp, P.T. Hammond, Fast Ion Conduction in Layer-By-Layer Polymer

Films, Chem. Mater. 15 (2003) 1165–1173. https://doi.org/10.1021/cm020945a.

[32] Y. Akgöl, C. Cramer, C. Hofmann, Y. Karatas, H.-D. Wiemhöfer, M. Schönhoff, Humidity-Dependent DC Conductivity of Polyelectrolyte Multilayers: Protons or Other Small Ions as Charge Carriers?, Macromolecules. 43 (2010) 7282–7287. https://doi.org/10.1021/ma1012489.

[33] Y. Choi, H. Kim, J. Yang, S.W. Shin, S.H. Um, S. Lee, M.S. Kang, J.H. Cho, Proton-Conductor-Gated MoS2 Transistors with Room Temperature Electron Mobility of >100 cm2 V-1 s-1, Chem. Mater. 30 (2018) 4527–4535. https://doi.org/10.1021/acs.chemmater.8b00568.

[34] J.H. Choi, W. Xie, Y. Gu, C.D. Frisbie, T.P. Lodge, Single ion conducting, polymerized ionic liquid triblock copolymer films: High capacitance electrolyte gates for N-type transistors, ACS Appl. Mater. Interfaces. 7 (2015) 7294–7302. https://doi.org/10.1021/acsami.5b00495.

[35] A. Malti, E.O. Gabrielsson, M. Berggren, X. Crispin, Ultra-low voltage air-stable polyelectrolyte gated n-type organic thin film transistors, Appl. Phys. Lett. 99 (2011) 1–4. https://doi.org/10.1063/1.3626587.

[36] J. Jiang, Q. Wan, Q. Zhang, Transparent junctionless electric-double-layer transistors gated by a reinforced chitosan-based biopolymer electrolyte, IEEE Trans. Electron Devices. 60 (2013) 1951–1957. https://doi.org/10.1109/TED.2013.2258922.

[37] J. Jiang, M.A. Kuroda, A.C. Ahyi, T. Isaacs-Smith, V. Mirkhani, M. Park, S. Dhar, Chitosan solid electrolyte as electric double layer in multilayer MoS2 transistor for low-voltage operation, Phys. Status Solidi Appl. Mater. Sci. 212 (2015) 2219–2225. https://doi.org/10.1002/pssa.201532284.

[38] K. Ariga, J.P. Hill, Q. Ji, Layer-by-layer assembly as a versatile bottom-up nanofabrication technique for exploratory research and realistic application, Phys. Chem. Chem. Phys. 9 (2007) 2319–2340. https://doi.org/10.1039/b700410a.

[39] E. Haladjova, G. Mountrichas, S. Pispas, S. Rangelov, Poly(vinyl benzyl trimethylammonium chloride) Homo and Block Copolymers Complexation with DNA, J. Phys. Chem. B. 120 (2016) 2586–2595. https://doi.org/10.1021/acs.jpcb.5b12477.

[40] G. Decher, Fuzzy Nanoassemblies : Toward Layered Polymeric Multicomposites, Science (80-.). 277 (1997) 1232–1237. doi: 10.1126/science.277.5330.1232.

[41] J.E. Yoo, K.S. Lee, A. Garcia, J. Tarver, E.D. Gomez, K. Baldwin, Y. Sun, H. Meng, T.Q. Nguyen, Y.L. Loo, Directly patternable, highly conducting polymers for broad applications in organic electronics, Proc. Natl. Acad. Sci. U. S. A. 107 (2010) 5712–5717. https://doi.org/10.1073/pnas.0913879107.

[42] T. Chen, M. Li, J. Liu, π-π Stacking Interaction: A Nondestructive and Facile Means in Material Engineering for Bioapplications, Cryst. Growth Des. 18 (2018) 2765–2783. https://doi.org/10.1021/acs.cgd.7b01503.

[43] Z. Zhao, W. Cai, Z. Xu, X. Mu, X. Ren, B. Zou, Z. Gui, Y. Hu, Multi-role p-styrene sulfonate assisted electrochemical preparation of functionalized graphene nanosheets for improving fire safety and mechanical property of polystyrene composites, Compos. Part B Eng. 181 (2020) 107544. https://doi.org/10.1016/j.compositesb.2019.107544.

[44] B.S. Kim, J. Choi, K.H. Min, H. Choi, H.-H. Park, S.-H. Baeck, S.E. Shim, Y. Qian, Fabrication of robust and superinsulating polystyrene-fortified silica aerogels via π–π interactions: Beyond styrofoam, Eur. Polym. J. 200 (2023) 112476. https://doi.org/10.1016/j.eurpolymj.2023.112476.

[45] A.S. Aglikov, T.A. Aliev, M. V. Zhukov, A.A. Nikitina, E. Smirnov, D.A. Kozodaev, M.I. Nosonovsky, E. V. Skorb, Topological Data Analysis of Nanoscale Roughness of Layer-by-Layer Polyelectrolyte Samples Using Machine Learning, ACS Appl. Electron. Mater. (2023). https://doi.org/10.1021/acsaelm.3c01358.

[46] R.F.M. Lobo, M.A. Pereira-da-Silva, M. Raposo, R.M. Faria, O.N. Oliveira, The morphology of layer-by-layer films of polymer/polyelectrolyte studied by atomic force

microscopy, Nanotechnology. 14 (2003) 101–108. https://doi.org/10.1088/0957-4484/14/1/322.

[47] M. Olszyna, A. Debrassi, C. Üzüm, L. Dähne, Label-Free Bioanalysis Based on Low-Q Whispering Gallery Modes: Rapid Preparation of Microsensors by Means of Layer-by-Layer Technology, Adv. Funct. Mater. 29 (2019) 1–7. https://doi.org/10.1002/adfm.201805998.

[48] J. Brandrup, E.H. Immergut, E.A. Grulke, Polymer Handbook, Fourth Edition, John Wiley & Sons, 1989. https://doi.org/https://doi.org/10.1002/actp.1990.010410614.

[49] Y. Lvov, K. Ariga, T. Kunitake, I. Ichinose, Assembly of Multicomponent Protein Films by Means of Electrostatic Layer-by-Layer Adsorption, J. Am. Chem. Soc. 117 (1995) 6117–6123. https://doi.org/10.1021/ja00127a026.

[50] E. Tjipto, J.F. Quinn, F. Caruso, Assembly of multilayer films from polyelectrolytes containing weak and strong acid moieties, Langmuir. 21 (2005) 8785–8792. https://doi.org/10.1021/la051197h.

[51] S. Dodoo, R. Steitz, A. Laschewsky, R. von Klitzing, Effect of ionic strength and type of ions on the structure of water swollen polyelectrolyte multilayers, Phys. Chem. Chem. Phys. 13 (2011) 10318. https://doi.org/10.1039/c0cp01357a.

[52] Q. Thiburce, A.J. Campbell, Low-Voltage Polyelectrolyte-Gated Polymer Field-Effect Transistors Gravure Printed at High Speed on Flexible Plastic Substrates, Adv. Electron. Mater. 3 (2017). https://doi.org/10.1002/aelm.201600421.

[53] L. Herlogsson, Y.Y. Noh, N. Zhao, X. Crispin, H. Sirringhaus, M. Berggren, Downscaling of organic field-effect transistors with a polyelectrolyte gate insulator, Adv. Mater. 20 (2008) 4708–4713. https://doi.org/10.1002/adma.200801756.

[54] J.B. Schlenoff, H. Ly, M. Li, Charge and mass balance in polyelectrolyte multilayers, J. Am. Chem. Soc. 120 (1998) 7626–7634. https://doi.org/10.1021/ja980350+.

[55] D.M. Delongchamp, P.T. Hammond, Highly ion conductive poly(ethylene oxide)-based solid polymer electrolytes from hydrogen bonding layer-by-layer assembly, Langmuir. 20 (2004)

5403–5411. https://doi.org/10.1021/la049777m.